Role of Surface Area on the Performance of Iron Nickel Nanoparticles for the Oxygen Evolution Reaction (OER)

P. Acharya^{1,a}, J.N. Burrow^{1,a}, M. Abolhassani^a, L.F. Greenlee^{a,*}

^a Ralph E. Martin Department of Chemical Engineering, University of Arkansas, Fayetteville, AR 72701, USA

¹ These authors contributed equally to this manuscript.

*Corresponding Author: greenlee@uark.edu; 610-507-6390

Iron-nickel bimetallic electrocatalysts have recently emerged as some of the best candidates for the oxygen evolution reaction (OER) in alkaline electrolyte. Understanding the effects of composition and morphology of iron-nickel nanoparticles is crucial for optimization and enhanced electrocatalyst performance. Both physical surface area and electrochemical surface area (ECSA) are functions of morphology. In this study, three different iron-nickel nanoparticle catalysts were synthesized. The three catalysts were varied based on morphology (alloy versus core-shell) and composition (high versus low stabilizer concentration). Brunauer-Emmett-Teller (BET) surface area analysis was conducted on the synthesized iron-nickel nanoparticles using a physisorption analyzer while electrochemical impedance spectroscopy (EIS) was employed to quantify the ECSA by capacitance. Comparison of ECSA and BET results to electrocatalyst overpotential suggests both available surface area and nanoparticle morphology play roles in electrocatalytic activity.

Introduction

Sustainable production of clean energy represents one of the most pressing challenges facing modern scientists. Hydrogen is considered a promising alternative fuel due to its high specific energy density (1). Hydrogen-powered fuel cells or direct combustion processes produce no greenhouse gases (2, 3). In addition, hydrogen is an important feedstock for industrial processes such as ammonia synthesis. Splitting water into its component gases is possible by a variety of processes and represents a viable method for hydrogen production. Water electrolysis, one of these processes, occurs when sufficient potential is applied to an electrochemical cell. The electrochemical decomposition of water into hydrogen and oxygen involves two half-reactions, the hydrogen evolution reaction (HER) and the oxygen evolution reaction (OER). Comparatively, the kinetics of OER are more sluggish than HER due to a four-electron transfer mechanism, which contributes to a slowing down of the overall water electrolysis reaction (2, 4). Increasing the efficiency of OER, therefore, has broad implications for clean hydrogen production.

Many catalyst materials have been well-studied and found to show considerable activity for oxygen evolution. Nickel-based catalysts have garnered considerable attention as nickel is an abundant metal with intrinsic activity for OER (5-7). Trotochaud et al. discovered that unintentional iron doping into a nickel hydroxide lattice increased the observed OER current density by at least an order of magnitude (8). Other researchers have

also concluded that bimetallic iron-nickel oxides or hydroxides are among the most active materials for OER (1, 3, 9).

An essential design component for an OER catalyst is to maximize the available surface area, which is expected to play a crucial role in catalytic activity. With higher surface area, more active sites on the catalysts are available for reactions to take place, which in turn can increase the kinetics of the reaction (4, 10-12). For electrocatalysts, an analogous electrochemical surface area (ECSA) exists. The ECSA describes the electrochemically accessible active surface area and can reveal electrocatalytic properties of the material (13-16). Importantly, Bau et al. concluded that ECSA was the primary factor governing OER kinetics for nickel-iron oxide nanocrystals (13).

A related and interesting aspect in the study of active OER nanocatalysts is the presence of ligands used in stabilization of metal precursors during the synthesis of nanocatalysts. Polyvinylpyrrolidone (PVP) is a common stabilizer used in nanoparticle synthesis, as it is known to prevent nanoparticle coalescence and thus allows the stable formation of smaller and similar-sized nanoparticles (17). No clear consensus has been formed in the scientific literature regarding the effects of PVP in the performance of catalysts. Lu et al. remarked that the presence of PVP caused a steep decline in the catalytic performance of silver nanorods, and similar results were observed by Long et al. with platinum nanoparticles (18, 19). However, Tong et al. reported that PVP introduced additional reaction pathways (20). Thus, ligand-metal interaction studies are also critical in catalyst optimization.

In this work, three types of bimetallic iron-nickel oxide/hydroxide nanoparticles were studied: Fe₁Ni₅ (low PVP, alloy) referred to as "LA"; Fe₁Ni₅ (high PVP, alloy) referred to as "HA"; and Fe₁Ni₅ (high PVP, core-shell) referred to as "HCS". These nanomaterials were synthesized and compared using characterization techniques including Brunauer-Emmett-Teller (BET) surface area analysis and electrochemical impedance spectroscopy (EIS). Electrochemical performance was evaluated and is reported as the OER overpotential (η, V vs. Hg/HgO) at 10 mA/cm². All three nanoparticle materials are expected to have surfaces comprised primarily of iron-incorporated nickel hydroxide; compositional and morphological characterization data and results are reported elsewhere (1, 2).

Experimental Section

Materials

ACS grade chemicals were purchased from commercial vendors. Iron sulfate heptahydrate (FeSO₄*7H₂O), nickel chloride hexahydrate (NiCl₂*6H₂O), sodium borohydride (NaBH₄), methanol, Nafion®, aminotris(methylene phosphonic acid) (ATMP), and polyvinylpyrrolidone (MW = 40,000 g/mol) (PVP40000) were used without any alteration. Potassium hydroxide was also purchased from a commercial vendor, and purification of 1 M KOH solutions was performed before use (8). A Millipore Milli-Q® Integral water purification system in the lab supplied ultrapure water.

Synthesis of Nanoparticles

All three nanoparticles – LA, HA, HCS – were synthesized under atmospheric pressure and room temperature. 18.2 M Ω H₂O was used as the solvent for all the synthesis solutions. For alloy nanoparticles (NPs), FeSO₄*7H₂O and ATMP were added together at a molar ratio of Fe:ATMP = 1:0.05 and hand-mixed for a short time. Independently, NiCl₂*6H₂O

and PVP40000 were hand-mixed together. For HA and LA, the molar ratios of nickel to PVP40000 used were Ni:PVP = 1:0.005 and Ni:PVP = 1:0.001, respectively. The mixture of iron salt plus ATMP and the mixture of nickel salt plus PVP were then added to a threenecked round bottom borosilicate flask. The contents of the flask underwent argon bubbling for 15 minutes while stirred on an orbital shaker at 100 rpm. A NaBH₄ solution was then added dropwise with a syringe to chemically reduce the metal precursors into NPs. The ratio of metal to borohydride was (mol metal:mol NaBH₄ = 1:2.2). Excess NaBH₄ accounts for the side reaction that occurs between water molecules and borohydride (21). The flask was placed under vacuum for 15 minutes on an orbital shaker and rotated at 100 rpm. The vacuum step removes the hydrogen gas formed as a byproduct of the reaction between NaBH₄ and the metal precursors. After the vacuuming process, the NP solution was transferred to a 50 mL centrifuge tube and centrifuged. The supernatant was decanted, and the NPs were re-suspended in methanol. Fe@Ni core-shell nanoparticles were synthesized in a similar fashion by first reducing iron to form iron nanoparticles and then introducing the nickel-stabilizer mixture (mol Ni:mol PVP = 1:0.005), which coats each iron nanoparticle with nickel through galvanic displacement of the iron metal atoms by the nickelous cations (1). This synthesis technique is summarized in Figure 1 below. A basis of 1 g/L of Fe was used in calculations for all three NPs.

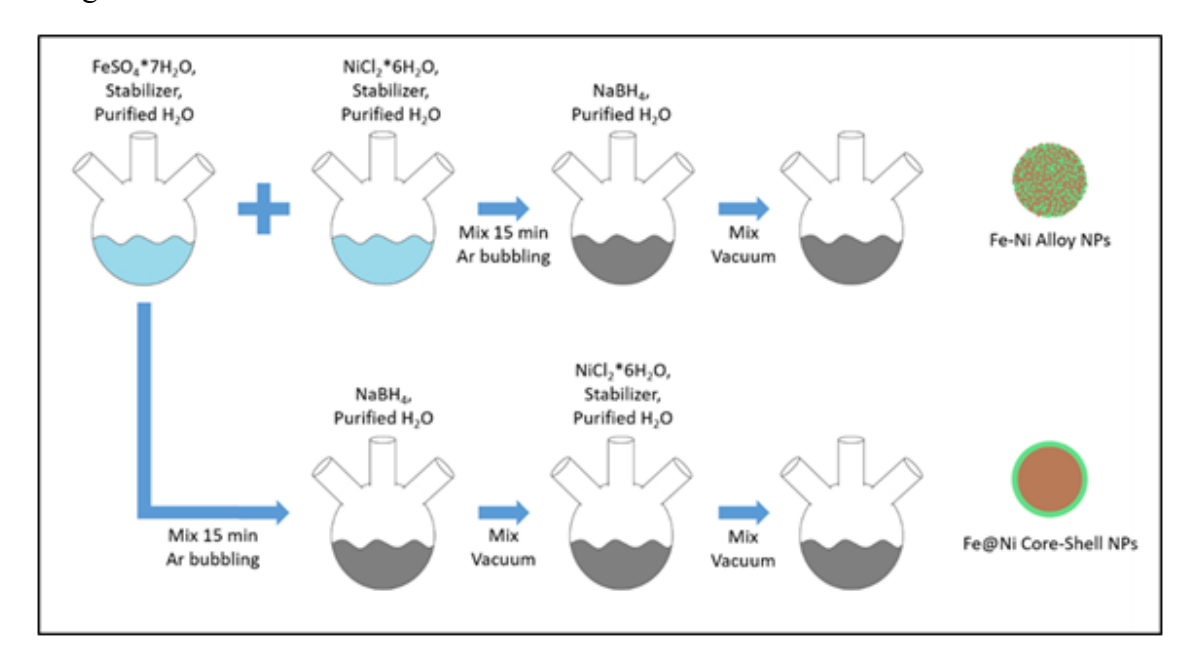


Figure 1: Schematic of alloy and core-shell FeNi NP synthesis.

Physical Surface Area Measurements

BET analysis was used to determine the physical surface area of each material. NP solutions were centrifuged, decanted, and placed under a fume hood to air dry overnight. Residual adsorbates were removed by degassing for 21 hours at 120°C. These conditions were selected in correspondence with thermogravimetric analysis (TGA) data previously reported for materials with similar metal-ligand interactions (22). A nitrogen adsorption isotherm was measured at 77 K for each nanoparticle sample, and multi-point BET analysis was performed with a Quantachrome Autosorb-iQTM.

ECSA Measurements

Potentiostatic electrochemical impedance spectroscopy (EIS) was employed to calculate ECSA. Measurements were performed with a potentiostat (Gamry Reference 3000) in a stationary three-electrode cell setup. A glassy carbon (GC) electrode (5mm dia., Pine) was used as the working electrode; a graphite rod was used as the counter electrode; and Hg/HgO was used as the reference electrode. The electrolyte solution used was purified 1M KOH. The purification process for KOH was done by following a procedure outlined in the literature by Trotochaud et. al (8). NPs were mixed with an ionomer (Nafion®) at a mass ratio of 30:1 (g NP:g Nafion) to form an ink. The catalyst was applied to the working electrode at a mass loading of around 500 μ g/cm² by the dropcasting method. Impedance spectra were measured at two different potentials: 0V and 0.52V vs Hg/HgO, as employed by Batchellor et al. (6). The amplitude of the sinusoidal wave was 10 mV, and the frequency range was from 0.1 Hz to 100 KHz.

Electrocatalyst Performance

Each nanoparticle sample was evaluated for OER performance via cyclic voltammetry (CV) experiments in the same experimental setup as described for EIS measurements. A series of CVs was obtained at a scan rate of 20 mV/sec, and the overpotential, η , was determined by subtracting the theoretical OER potential (E° = 1.23 V vs. RHE) from the measured potential at 10 mA/cm² (normalization is based on electrode geometric surface area) after converting the potential measurements from the experimental Hg/HgO reference electrode to the relative hydrogen electrode. Measured potentials were corrected for internal resistance as measured with EIS under open circuit potential.

Results and Discussion

Through BET analysis of nitrogen physisorption measurements for physical surface area (Figure 2), HA was found to have the largest surface area of the materials studied at 95.976 m²/g, followed by HCS, which had a surface area of 88.11 m²/g. LA had the lowest measured surface area of the three synthesized nanoparticle materials, with a value of 54.53 m²/g. LA nanoparticles were synthesized with the lowest amount of PVP (Ni:PVP = 1:0.001) among the three nanocatalysts. In comparison, both HCS and HA nanoparticles were synthesized with a nominal ratio of Ni:PVP = 1:0.005. The lower amount of PVP used during LA nanoparticle synthesis appears to have resulted in a significant decrease in the measured surface area. This decrease in measured surface area is possibly the result of increased agglomeration of the nanoparticles and therefore a reduction in the physically accessible surface area for nitrogen adsorption. In addition, the LA nanoparticles may have a larger average particle diameter, which would reduce the surface area per unit mass. The ratio of ligand stabilizer to metal precursor is known to impact both nanoparticle size and nanoparticle agglomeration in nanoparticle synthesis, and both effects need to be further investigated.

At the higher PVP concentration tested, both HA and HCS nanoparticles resulted in increased measured surface area compared to LA. It is likely that the increase in the PVP concentration during nanoparticle synthesis had a direct impact on this increase in measured surface area. Interestingly, the measured surface area of the HA nanoparticles is slightly larger than that of the HCS nanoparticles. Differences in particle diameter may contribute to this difference, but incomplete deposition of the nickel precursor may also contribute to a lower measured surface area for HCS nanoparticles. In Candelaria et al. (1), we reported that Fe@Ni core-shell nanoparticles synthesized at a theoretical precursor composition of Fe₁Ni₁ were experimentally determined to contain a bulk composition of

Fe_{3.2}Ni₁. These results, along with un-reported measurements of remaining nickel salt precursor in the decanted nanoparticle synthesis supernatant, demonstrate that only a portion of the nickel displaces iron metal atoms at the iron nanoparticle surface. This result may also result in a lower amount of PVP deposition on the surface and resulting differences in both nanoparticle size and nanoparticle agglomeration. Overall, the relationship between measured physical surface area and nanoparticle synthesis parameters is important to understand and further investigation will explore delineation of the roles of nanoparticle size, nanoparticle agglomeration, and nanoparticle morphology.

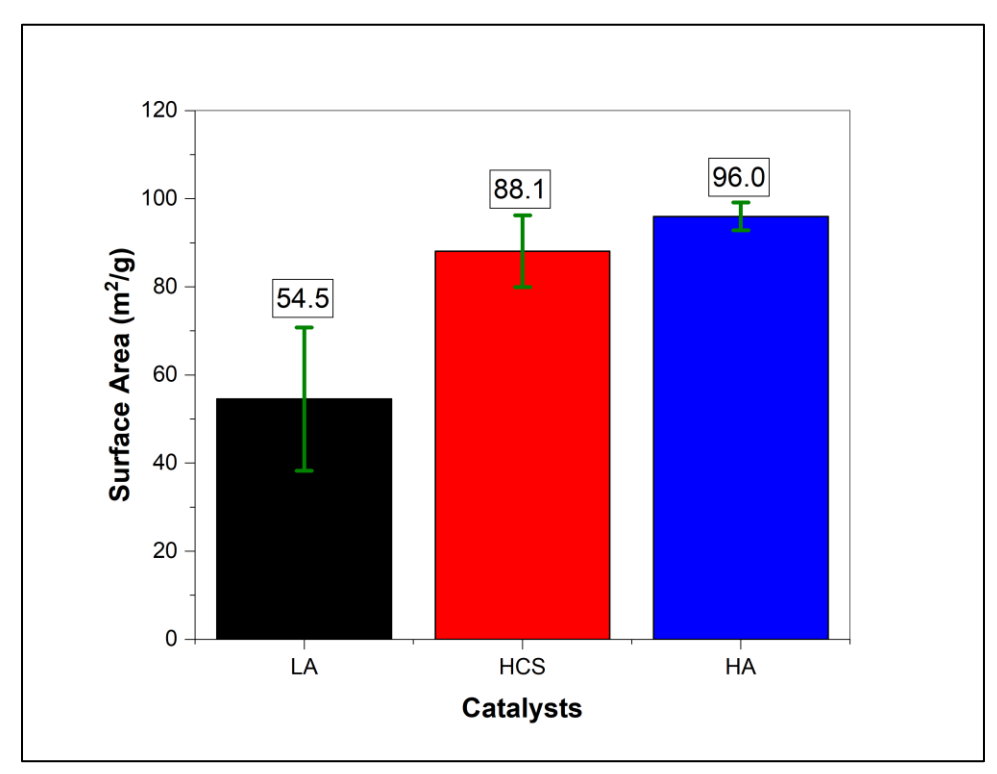


Figure 2. BET measurements of physical surface area.

To determine ECSA, impedance spectra were fit to a modified Randles circuit as shown in Figure 3 below. A pure capacitor was replaced with a constant phase element (CPE) as employed by McCrory et. al (7).

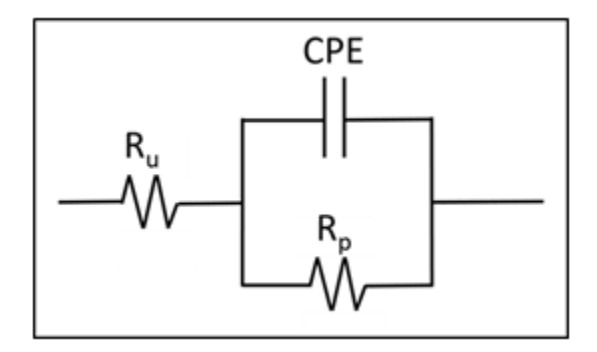


Figure 3. Randles circuit modified with R_u (uncompensated resistance), R_p (polarization resistance), and CPE (constant phase element) used for fitting.

The capacitance of the double layer formed in solution at the surface of each nanoparticle material was calculated using Equation 1 (23).

$$C_{\rm dl} = \frac{(Y_0 * R_p)^{\left(\frac{1}{\alpha}\right)}}{R_p}$$
 [Eqn. 1]

 C_{dl} is the capacitance of the double layer (F), Y_0 is a parameter that relates to the magnitude of capacity (S*s $^{\alpha}$), R_p is the polarization resistance connected in parallel with the constant phase element (CPE), and α is a dimensionless exponent that relates to inhomogeneity of the surface. C_{dl} values were calculated using EChem Analyst software.

ECSA can be determined from the capacitance of the double layer by normalizing C_{dl} with the specific capacitance (C_s). Previously reported values for specific capacitance of nickel and iron oxides in 1M KOH suggest a value around 0.04 mF cm⁻² (7). The measured ECSA of a clean GC electrode used in our experiments was calculated to be approximately 1.6 cm² and 0.9 cm² at 0V and 0.52V vs. Hg/HgO, respectively. ECSA values of all three nanocatalysts at two different potentials, 0V vs Hg/HgO and 0.52V vs Hg/HgO, are plotted in Figure 4. At 0V vs Hg/HgO, ECSA values of the three nanoparticles are quite similar and were within the range of 0.5 – 1.2 cm². These results closely match the ECSA obtained for the clean GC electrode. At 0.52V vs Hg/HgO, the measured ECSA for LA nanoparticles was not significantly greater than the ECSA acquired at 0V. However, for HCS and HA nanoparticles, ECSA values obtained at 0.52V increased by approximately 4 and 8 times, respectively, above those acquired at 0V.

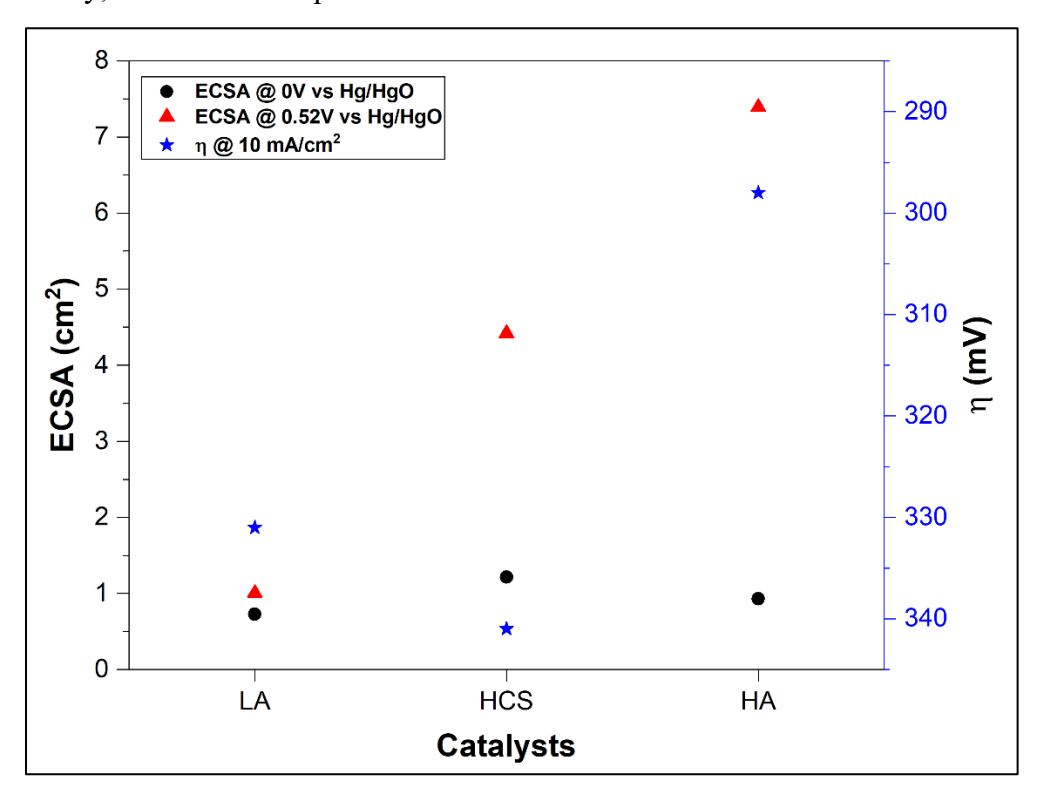


Figure 4. Calculated ECSA values for each material at 0V and at 0.52V vs. Hg/HgO, as well as measured overpotential (η) at 10 mA/cm².

The results of these ECSA experiments closely mirror the outcome of a similar set of experiments conducted by Batchellor et al. (14). In their study, Batchellor et al. (14) demonstrated for a series of iron-nickel hydroxide films that when EIS is used to measure ECSA at any potential below the nickel redox potential, the ECSA measurement is reflective of the working electrode material, rather than the iron-nickel catalyst. At

potentials below the nickel redox potential, nickel is in a nickel hydroxide phase, which is non-conductive. Above the nickel redox potential, nickel hydroxide converts to nickel oxyhydroxide as the nickel oxidizes, and nickel oxyhydroxide is conductive. When ECSA is used to measure the electrochemically-active surface area of an insulating material, such as an iron-nickel hydroxide film, the film essentially does not contribute to electrochemical activity, and thus, the only accessible electrochemically active surface, and therefore, the measured capacitance, is the working electrode material itself. In other words, ECSA is not a valid technique to measure the surface area of insulating materials. While the work of McCrory et al. (16) presented an overall useful approach for benchmarking metal oxide OER catalysts, their approach failed to account for potential-dependent conductivity and potential regions of applicability for ECSA measurement. Our results corroborate the updated approach of Batchellor et al. (14), where potentiostatic ECSA must be used, and the applied potential must be selected based on potential regions of known conductivity.

Thus, at a potential of 0V vs. Hg/HgO, all of the iron-nickel nanoparticles tested in this study are not conductive, and the ECSA measured is that of the electrode itself (i.e., glassy carbon in the present study) and not the catalyst. At higher potential, ECSA values significantly increased for HCS and HA nanoparticles, which suggest that these two nanocatalysts became conductive, and the ECSA measured was that of the catalyst not the GC electrode. In the case of the LA nanoparticles, either 0.52V vs Hg/HgO was not high enough for the catalyst to be conductive or the sample had a very low ECSA. In these, and similar, iron-nickel bimetallic catalysts, the predominant phase is nickel hydroxide (Ni(OH)₂) (1, 3, 8, 14), which is not conductive. However, above the redox peak of nickel, nickel oxyhydroxide forms, which is conductive. Since the theoretical composition of these three samples is the same, and the redox peak of Ni²⁺/Ni^{3+/4+} is known to occur at 0.4-0.5 V vs. Hg/HgO, we would expect all three samples to be conductive at 0.52V. As a result, our data suggest that the role of the PVP ligand concentration during synthesis may play an important role in both the physical surface area and the electrochemically active surface area, as it appears that a lower PVP content used during nanoparticle synthesis resulted in a significantly lower ECSA. Further, differences in the ECSA results for HCS and HA nanoparticles also warrant further investigation to better understand how nanoparticle morphology (i.e., core-shell versus alloy) controls the electrochemically available and active surface area of iron-nickel nanoparticles.

In Figure 4, the OER overpotential (η) of each of the nanoparticle samples is also reported (scale is on the right y-axis). Generally, a lower measured overpotential suggests faster electrocatalyst kinetics and therefore a more active catalyst material. Interestingly, an increase in ECSA does not necessarily result in a reduction of the OER overpotential. The HCS nanoparticle electrocatalyst resulted in an OER overpotential of 341 mV, which is the highest measured overpotential of the three nanoparticle electrocatalysts. This result suggests that for our nanoparticle catalysts, ECSA can not be the only parameter used to predict electrocatalytic activity. Within the set of alloy nanoparticles, the HA nanoparticles resulted in both the highest ECSA and the lowest OER overpotential (298 mV), and the increase in ECSA with an increase in the PVP concentration used in nanoparticle synthesis seems to correlate to a decrease in OER overpotential. These results suggest that the amount of PVP ligand stabilizer used during synthesis is a critical parameter to study and understand to enable the tuning of this catalyst suite for optimal OER performance. In addition, the differences in OER overpotential observed for alloy versus core-shell morphology suggest other parameters must be identified and correlated to OER performance.

Conclusions

In this study, three nanoparticle materials (LA, HA, and HCS) were synthesized in an aqueous-based solution at atmospheric pressure and room temperature. The three nanoparticles were varied based on morphology (core-shell vs. alloy) and PVP to nickel molar ratio (low vs high). Both physical surface area and ECSA were measured for all three nanoparticle samples. LA, which had lower PVP ratio compared to HA and HCS, had the lowest surface area of the three nanoparticle types. LA also had the lowest ECSA value (@) 0.52V vs. Hg/HgO), while HA had both the highest surface area and ECSA value (@ 0.52V vs. Hg/HgO), followed by HCS. The results suggest that a lower amount of PVP could lead to higher coalescence of the particles and/or larger particle diameter, thus reducing the surface area. Also, there may be a direct relationship between the physical surface area and the ECSA of the nanocatalysts. Finally, measurements of OER overpotential demonstrate that HA is the most active for OER, with the lowest overpotential of 298 mV, while both LA and HCS have relatively high OER overpotentials of 331 mV and 341 mV, respectively. These results provide initial evidence that both morphology and ligand concentration play important roles in iron-nickel nanoparticle electrocatalytic activity for OER.

Acknowledgements

The authors gratefully acknowledge funding support for PA from the National Science Foundation, Division of Chemical, Bioengineering, Environmental, and Transport Systems (award # 1703827). JNB acknowledges the University of Arkansas Honors College Research Grant program for support.

References

- 1. S. L. Candelaria, N. M. Bedford, T. J. Woehl, N. S. Rentz, A. R. Showalter, S. Pylypenko, B. A. Bunker, S. Lee, B. Reinhart and Y. Ren, *ACS Catal.*, 7, 365 (2016).
- 2. L. F. Greenlee, P. Acharya and Z. Nelson, ECS Trans., 77, 25 (2017).
- 3. D. Friebel, M. W. Louie, M. Bajdich, K. E. Sanwald, Y. Cai, A. M. Wise, M.-J. Cheng, D. Sokaras, T.-C. Weng and R. Alonso-Mori, *J. Am. Chem. Soc.*, **137**, 1305 (2015).
- 4. L. Xu, Q. Jiang, Z. Xiao, X. Li, J. Huo, S. Wang and L. Dai, *Angew. Chem.*, **128**, 5363 (2016).
- 5. D. A. Corrigan, *J. Electrochem. Soc.*, **134**, 377 (1987).
- 6. A. Singh and L. Spiccia, Coord. Chem. Rev., 257, 2607 (2013).
- 7. L. Trotochaud and S. W. Boettcher, *Scripta Mater.*, **74**, 25 (2014).
- 8. L. Trotochaud, S. L. Young, J. K. Ranney and S. W. Boettcher, *J. Am. Chem. Soc.*, **136**, 6744 (2014).
- 9. M. W. Louie and A. T. Bell, *J. Am. Chem. Soc.*, **135**, 12329 (2013).
- 10. X. Yu and S. Ye, *J. Power Sourc.*, **172**, 145 (2007).
- 11. Z. Chen, D. Higgins, A. Yu, L. Zhang and J. Zhang, *Energy Environ. Sci.*, **4**, 3167 (2011).
- 12. H. Tanaka and M. Misono, Curr. Opin. Solid State Mater. Sci., 5, 381 (2001).
- 13. J. A. Bau, E. J. Luber and J. M. Buriak, ACS Appl. Mater. Inter., 7, 19755 (2015).
- 14. A. S. Batchellor and S. W. Boettcher, *ACS Catal.*, **5**, 6680 (2015).
- 15. M. B. Stevens, L. J. Enman, A. S. Batchellor, M. R. Cosby, A. E. Vise, C. D. Trang and S. W. Boettcher, *Chem. Mater.*, **29**, 120 (2016).
- 16. C. C. McCrory, S. Jung, J. C. Peters and T. F. Jaramillo, *J. Am. Chem. Soc.*, **135**, 16977 (2013).
- 17. K. M. Koczkur, S. Mourdikoudis, L. Polavarapu and S. E. Skrabalak, *Dalton Trans.*, **44**, 17883 (2015).
- 18. Y. Lu, Y. Wang and W. Chen, *J. Power Sourc.*, **196**, 3033 (2011).
- 19. N. V. Long, M. Ohtaki, M. Nogami and T. D. Hien, *Coll. Polym. Sci.*, **289**, 1373 (2011).
- 20. C. Susut, D.-J. Chen, S.-G. Sun and Y. J. Tong, *Phys. Chem. Chem. Phys.*, **13**, 7467 (2011).
- 21. N. Goldstein and L. F. Greenlee, *J. Nanopart. Res.*, **14**, 760 (2012).
- 22. S. Karna, S. Mishra, E. Gunapala, I. Dubenko, V. Malagareddy, G. Marasinghe and N. Ali, *J. Nanosci. Nanotechnol.*, **10**, 5879 (2010).
- 23. V. Jovic, Res. Solut. Resourc., Gamry Application Note (2003).